Cycle-resolved emissions analysis of polyfuel reciprocating engines via in-situ laser absorption spectroscopy

Kevin Schwarm, Nicolas Minesi, Barathan Jeevaretanam, Sarah Enayati, Tsu-Chin Tsao, R. Mitchell Spearrin

▶ **To cite this version:**

Kevin Schwarm, Nicolas Minesi, Barathan Jeevaretanam, Sarah Enayati, Tsu-Chin Tsao, et al.. Cycle-resolved emissions analysis of polyfuel reciprocating engines via in-situ laser absorption spectroscopy. Internal Combustion Engine ICE Forward Conference, ASME, Oct 2022, Indianapolis, IN, France. 10.1115/ICEF2022-88543 . hal-04123257

HAL Id: hal-04123257
https://hal.science/hal-04123257v1

Submitted on 21 Jun 2023

HAL is a multi-disciplinary open access archive for the deposit and dissemination of scientific research documents, whether they are published or not. The documents may come from teaching and research institutions in France or abroad, or from public or private research centers.

L'archive ouverte pluridisciplinaire **HAL**, est destinée au dépôt et à la diffusion de documents scientifiques de niveau recherche, publiés ou non, émanant des établissements d'enseignement et de recherche français ou étrangers, des laboratoires publics ou privés.

Proceedings of the ASME 2022
Internal Combustion Engine ICE Forward Conference
ICEF2022
October 16–19, 2022, Indianapolis, IN

ICEF2022-88543

CYCLE-RESOLVED EMISSIONS ANALYSIS OF POLYFUEL RECIPROCATING ENGINES VIA IN-SITU LASER ABSORPTION SPECTROSCOPY

Kevin K. Schwarm[1,*], Nicolas Q. Minesi[1], Barathan Jeevaretanam[1], Sarah Enayati[1], Tsu-Chin Tsao[1], R. Mitchell Spearrin[1]

[1]University of California, Los Angeles, Los Angeles, CA

ABSTRACT

A high-speed in-situ laser absorption sensor has been developed for cycle-resolved emissions analysis in the exhaust manifold of production-scale internal combustion engines. An in-line sensor module, using optical fiber-coupling of interband and quantum cascade lasers, targets the fundamental rovibrational absorption lines of carbon monoxide and nitric oxide near 5 µm in wavelength. The sensor module was integrated into a commercial EPA-certified natural gas spark-ignition generator operated at 3,300 rpm for measurements of exhaust pulse temperature, CO, and NO concentrations at a rate of 10 kHz. Novel high-temperature optomechanical design enabled in-stream sensor coupling near the exhaust valve with local gas temperatures up to ~1200 K and valve to sensor gas transit times on the order of milliseconds. Measurement results reveal high degrees of intra-cycle and cycle-to-cycle variations which are otherwise undetectable with standard emission gas analyzers. Sensor response to variations in fuel composition were evaluated by introduction of 1-10% NH_3 or H_2 into the natural gas fuel system. The effects of fuel blending on exhaust emissions of CO and NO were well-distinguished even at 1% volume fraction, and the sensor captured both intra-cycle and cycle-averaged emissions differences between the three fuel types. Measured concentrations of CO and NO ranged from 0.1-2.8% and 30-3500 ppm with detection limits of 0.07% and 26 ppm, respectively. The exhaust sensor presented here has potential for integration with real-time control systems to enable adaptive optimization of polyfuel internal combustion engines to meet the need for flexible, low-carbon, on-demand energy conversion.

Keywords: IC engines, emissions, natural gas, ammonia, hydrogen, intra-cycle, high-speed sensor

1. INTRODUCTION

Internal combustion (IC) engines are widely used for transportation but also provide efficient on-demand distributed electrical power in case of power outages. However, in these applications, gasoline or diesel fuel usage is slowly decaying owing to high carbon emissions. Policymakers have encouraged shifting towards natural gas (NG) because of its lower CO_2 emission factor; natural gas emits 25% less CO_2 than gasoline for the same heat release [1]. Natural gas engines are commercially available, but if tuned incorrectly for a given load or fuel blend, can suffer from poor performance and cycle-to-cycle variability caused by combustion instabilities, especially when operating fuel-lean for increased efficiency [2]. Further reducing engine carbon footprint can be achieved by employing renewable or carbon-free fuels, such as ammonia (NH_3) and hydrogen (H_2) [3]. However, IC engines running on neat NH_3 or NH_3/H_2 mixtures present some disadvantages, including potentially increased NO_x emissions and limited availability relative to their natural gas counterparts.

Stable combustion of pure NH_3 in IC engines is difficult to achieve, and experiments in research engines tend to use the addition of H_2 to enhance ignition performance. Mercier et al. showed that partial on-board cracking of pure NH_3 (to form H_2) improved the engine stability, even at low loads [4]. When blending 5–10% H_2 in NH_3 by volume, indicated thermal efficiencies of approximately 36% near stoichiometric air-to-fuel ratio operation were achieved [4, 5], comparable to typical efficiencies of NG engines [2]. Recent progress demonstrated that brake-specific CO_2 emissions could be reduced by 28% by blending 50% NH_3 by volume in natural gas while maintaining stable performance in a 6-cylinder engine originally employed for city buses [6]. With fixed timing of ignition and fuel injection, Moreno et al. found that H_2 addition to CH_4 decreased the brake-specific CO_2 emissions but increased the brake-specific NO emissions, although this could be mitigated by running the engine at leaner conditions [7]. Blending NH_3 and H_2 in natural gas represents a potential strategy for easing transitions to carbon-free combustion while also providing engine operators with the flexibility to quickly respond to new policies and fluctuations in fuel availability / cost-efficiency, which often occur on faster timescales than those of engine or generator replacement. Thus, there is a

*Corresponding author: kschwarm@g.ucla.edu
Documentation for `asmeconf.cls`: Version 1.30, June 9, 2023.

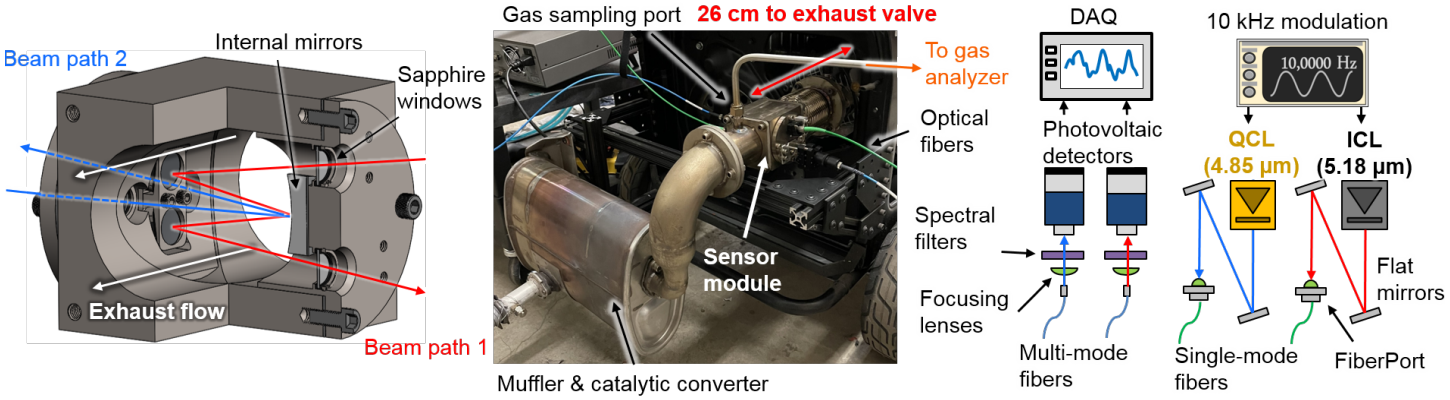

FIGURE 1: *LEFT*: DESIGN MODEL OF EXHAUST SENSOR MODULE WITH OPTICAL ARRANGEMENT FOR MULTI-PATH, MULTI-PASS BEAM GEOMETRY. *MIDDLE*: SENSOR INCLUDING OPTICAL FIBERS AND KINEMATIC MOUNTING SYSTEM INSTALLED WITH THE MODIFIED EXHAUST PIPE ON THE HONDA EU7000IS ELECTRICITY GENERATOR. *RIGHT*: OPTICAL BREADBOARD SETUP WITH LIGHT SOURCES AND OPTICS.

need to improve the performance and adaptability of IC engine architectures that can sustain reliable and efficient operation with a wide variety of low-carbon fuel compositions.

IC engine operation with varying load, RPM, and fuel composition is well established, with a variety of methods available that aid the implementation of these novel fuels. For instance, variable spark timing is essential to account for the wide range of ignition delays encountered in NH_3/H_2 blends [5]. Further optimization can be achieved using variable valve actuation (VVA) systems that can adjust one or several parameters of the valve lift profile (e.g., amplitude, duration, and timing). Among the several VVA types explored thus far, the camless VVA system provides superior control flexibility of the entire valve lift profile [8]. For real-time engine optimization in response to varying fuel-blend composition or user demand, spark timing and valve actuation must heavily rely on feedback control informed by sensors which monitor engine performance and emissions in the exhaust manifold. If fed with low-latency intra-cycle data, the camless concept can rapidly adapt ignition, fuel, and valve control to respond to higher-frequency (>Hz) combustion behaviors. Such an increased level of performance can only be achieved if the VVA system is paired with sensors that are fast (>kHz), quantitative, and capable of reliable operation in the harsh conditions of an IC engine exhaust manifold. In addition to measurement time resolution, the coupling of such sensors as close as possible to the combustion source, such as with minimal distance between the exhaust valve and an exhaust gas sensor, is critical to fast control.

Exhaust measurements can be performed with well-established gas analyzers, which typically include electro-chemical (EC) sensors, non-dispersive infrared (NDIR), and flame ionization detectors (FID). Electro-chemical sensors are cheap, low power, and compact, but struggle in species sensitivity and selectivity, especially when faced with a moist high-temperature environment [9]. For this reason, the exhaust gas typically must be treated (usually desiccated to remove water) to prevent contamination or measurement interference. Non-dispersive infrared sensors for species detection rely on broadband light absorption for enhanced selectivity, although application is limited to certain strongly-absorbing species (e.g., CO_2). Moreover, routine calibration is also usually required for these sensors as their response tends to deviate with time and use. In addition to the aforementioned difficulties, typical time-resolution of conventional sensors is commonly on the order of seconds and cannot resolve the Hz- to kHz-scale processes of interest in combustion systems that can affect performance. Recently, some NDIR sensors have been developed for kHz-rate measurements of gas properties in IC engines [10, 11]. However, these systems still require calibration to be quantitative and are limited in their target species due to interference associated with poor spectral resolution.

This work details the development of an in-situ exhaust manifold sensor for time-resolved measurement of exhaust gas properties in production-grade IC engines. The work presented here is part of a broader effort to provide rapid detection and feedback of regulated emissions to a camless VVA system to offer efficient fuel flexibility. The sensor is based on time-resolved laser absorption spectroscopy, which is particularly well-suited to this application owing to its calibration-free, quantitative, and high temporal resolution capability up to and above kHz measurement rates. A high-temperature fiber-coupled sensor module enables close coupling to the engine exhaust valve to access combustion exhaust gases immediately after leaving the cylinder. This close-coupled approach reduces sensor latency and increases the quantitative value in measured gas properties and their connection to the in-cylinder combustion processes. The high temporal response reveals more granular emissions evolution by tracking both cycle-to-cycle and intra-cycle variation. We demonstrate the capabilities of this sensor by performing in-situ measurements of gas temperature, carbon monoxide, and nitric oxide in the exhaust pipe of an EPA-certified Honda GX390T2 four-stroke engine, see Fig. 1, operating on natural gas (NG) and low-carbon fuel blends incorporating NH_3 and H_2 (up to 10% volume fraction). The high-temperature durability of the sensor coupled with

a large dynamic range resulted in cycle-resolved measurements revealing significant combustion inconsistencies and differences in emissions among the various fuel blends, enabling new opportunities for further optimization by incorporating VVA with real-time control.

2. SENSOR METHODOLOGY

2.1 Laser Absorption Spectroscopy

Laser absorption spectroscopy (LAS) is an optical diagnostic technique that has been used extensively for quantitative analysis of combustion gases, and detailed discussions of the relevant theory can be found in the literature [12]. In scanned-wavelength direct absorption LAS, a narrow-linewidth laser is tuned across wavelengths corresponding to absorption transitions of target molecules. The laser output beam is directed through the flow of interest, and the transmitted light intensity is recorded on a photodetector. The attenuation of the laser radiation due to molecular absorption can be related to gas properties through the Beer-Lambert Law, shown in Eq. 1:

$$A = \int_{-\infty}^{\infty} \alpha(\nu) d\nu = \int_{-\infty}^{\infty} -\ln\left(\frac{I_t}{I_0}\right)_{\nu} d\nu = X_i S(T) P L \qquad (1)$$

I_0 represents the incident laser output intensity during modulation while I_t represents the measured transmitted intensity after the light passes through the absorbing medium. Spectral absorbance $\alpha(\nu)$ across the absorbing region is calculated with these recorded signals, where ν [cm^{-1}] is the wavenumber. By integrating over a single spectral line, one can calculate an absorbance area A [cm^{-1}] which can be related to absorbing species mole fraction X_i through Eq. 1 with the knowledge of temperature-dependent linestrength $S(T)$ [cm^{-2}·atm^{-1}] (from spectral databases), gas pressure P [atm] (measured or known), and absorption pathlength L [cm] (known from system design).

Gas temperature, when unknown, can be calculated using a two-line thermometry technique [13]. By taking the ratio R of the absorbance areas of two lines (A and B) from a single species, as in Eq. 2, the dependence on pressure, pathlength, and concentration in the Beer-Lambert law are removed, and this ratio becomes solely a function of temperature. To achieve a sensitive temperature measurement, the two lines should have differing dependencies on temperature and this can be achieved by targeting transitions with a large difference in lower state energy.

$$R = \frac{A_A}{A_B} = \frac{S_A(T)}{S_B(T)} = f(T) \qquad (2)$$

Therefore, the simultaneous measurement of two absorption transitions of the same species provides a straightforward measurement of gas temperature and species concentration. By spectrally-resolving these individual absorption transitions, this method is species-specific, calibration-free, and quantitative. Notably, LAS is readily configurable in non-intrusive, in-situ optical arrangements [12], so high-precision quantitative measurements are possible with minimal disruption to the flow of combustion gases and overall packaging of production IC engines.

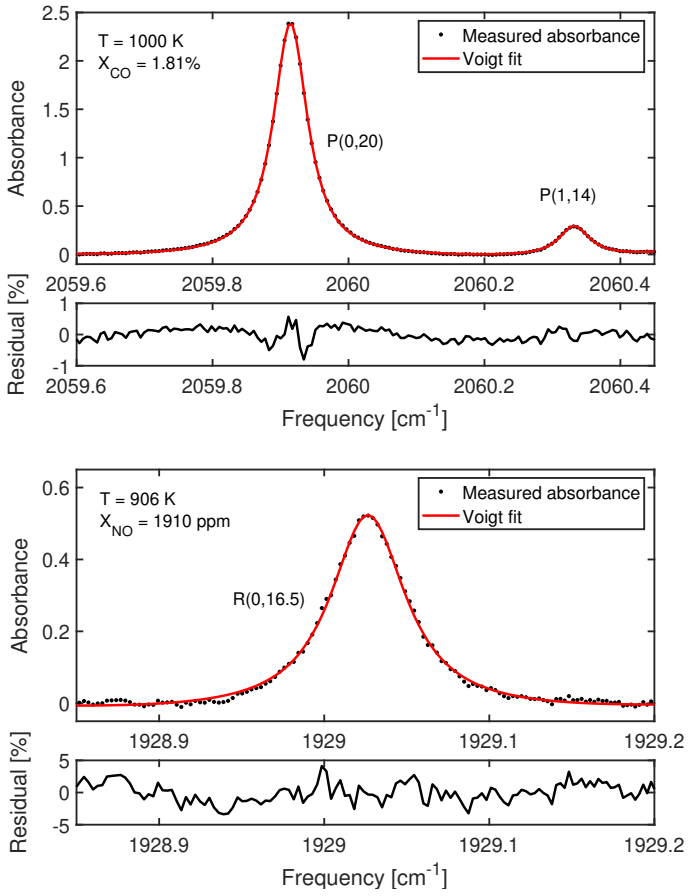

FIGURE 2: REPRESENTATIVE ABSORPTION SPECTRA OF CARBON MONOXIDE *(TOP)* AND NITRIC OXIDE *(BOTTOM)* MEASURED IN THE ENGINE EXHAUST AND FITTED BY VOIGT LINESHAPES.

2.2 Spectroscopic Approach

The emergence of mid-infrared photonics has extended applications of LAS to cover the fundamental rovibrational absorption bands of important combustion species [12]. The inherent high absorption strength of these bands enables increased sensitivity for trace gas detection and use in harsh environments, which is advantageous for deployment in IC engine exhaust systems. Carbon monoxide (CO) and nitric oxide (NO), whose fundamental bands lie near 5 µm, are the selected species for detection in the IC engine exhaust, as these species both serve as markers of combustion performance and are regulated as exhaust emissions [14]. Furthermore, recent studies into polyfuel combustion involving natural gas, NH_3, and H_2 have highlighted CO and NO_x production as areas requiring further investigation to optimize in-cylinder combustion and facilitate use of these fuels in practical engines subject to emissions regulations [2, 4–7].

Figure 2 shows the target absorption transitions, selected for their absorption strength and lack of spectral interference by other absorbing species (e.g., H_2O, CO_2). CO detection is accomplished through simultaneous measurement of the P(0,20) and P(1,14) transitions near 2059.9 cm^{-1} and 2060.3 cm^{-1}, respectively. A quantum cascade laser (QCL, ALPES Lasers) near

4.85 µm is current-modulated to scan both transitions at a rate of 10 kHz. A Voigt lineshape function is simultaneously fitted to each transition (see Fig. 2) to extract the absorbance areas which are subsequently used to infer gas temperature and CO mole fraction through Eqs. 1 & 2. This line pair has been demonstrated previously to provide precise measurement of temperature and CO mole fraction in convoluted combustion gases [15, 16]. The NO absorption transition selected for this application is the R(0,16.5) transition near 1929.0 cm^{-1}, which is similarly spectrally-resolved at a rate of 10 kHz with an interband cascade laser (ICL, Nanoplus) near 5.18 µm. After extracting absorbance area via Voigt lineshape fitting shown in Fig. 2, the NO mole fraction is calculated through Eq. 1 using the gas temperature determined from the CO spectrum. This absorption transition has also previously been measured with success in combustion and IC engine exhaust studies, validating its selection for this application [17, 18]. An exhaust gas pressure of 1 atm is assumed for the mole fraction calculation, and spectroscopic parameters used for extraction of temperature and mole fraction are taken from the HITEMP database, as well as a recent study by Almodovar et al. [19–21].

2.3 Optomechanical Sensor Design

The integration of laser absorption sensors in the exhaust system of a production IC engine faces practical challenges—to achieve intra-cycle resolution of the exhaust pulses, and to minimize sensor latency for feedback on combustion events, the sensing location must be as close to the exhaust valve as possible with minimal disturbance to the flow path. When applied to a continuously operating IC engine, this requires sensor operation at sustained high temperatures and vibration, presenting an exceptionally harsh environment for optics and photonics. Additionally, the sensor integration must be accomplished without compromising engine operation or performance.

The exhaust sensor module design is shown in Fig. 1 and is inspired by the work of Diemel et al. [18] with important distinctions enabling operation at higher temperatures. The stainless steel central body and removable port plugs form a compact module that houses the necessary optical elements around a central 50-mm bore to maintain smooth flow of the exhaust gases. The integrated optics form two orthogonal beam paths for simultaneous sensing with two light sources. Optical access is achieved with 1-mm thick, 12.7-mm diameter sapphire windows. The windows are secured in place with retaining rings and graphite gaskets. Silver-coated mirrors are mounted inside the module to facilitate multi-pass beam geometries to extend the optical pathlength and increase measurement sensitivity. The internal mirrors are secured with custom stainless steel clamps and graphite gaskets. The harsh exhaust environment precluded the use of high-temperature epoxies, so mechanical clamping mechanisms and graphite gaskets are used for all mounted optics to create a secure hold and stable alignment while simultaneously preventing fracture of the optics due to differential thermal expansion. This arrangement also allows for easy disassembly and reconfiguration of the optical paths or materials for alternative sensing strategies. The temperature uniformity within the measurement region was evaluated by translating a K-type thermocouple across the 50 mm bore at various load conditions. The steady-state radial temperature is uniform with the exception of a temperature drop-off starting 6 mm from the wall, with wall temperatures 10–13% lower than the measured core temperature depending on the load condition. This minor boundary temperature non-homogeneity has a negligible impact on the absorbance, and was therefore neglected in the LAS post-processing.

The first beam path (#1 in Fig. 1) employs a White-cell multi-pass arrangement, which facilitates long optical pathlengths in small volumes [22, 23]. This design features a system of three concave mirrors with matching radii of curvature corresponding to the separation distance. The laser beam enters on one side of the mirror arrangement, undergoes a series of internal reflections, and exits on the same side as the entrance through a second window. The number of internal reflections and achievable optical pathlength is adjustable and set by the angles of the pair of mirrors on the left in Fig. 1. The configuration shown has 12 internal passes for an aggregate 61.6 cm pathlength. The second beam path (#2 in Fig. 1) uses a simpler, dual-pass configuration with a single internal reflection and resulting aggregate optical pathlength of 11.9 cm. Input light for each path is delivered with single-mode solid-core InF_3 fibers and aspheric collimators to maintain 2-mm diameter Gaussian beams introduced to the multi-pass cells. An adjustable lens tube with a calcium fluoride plano-convex lens focuses the outgoing light into a 200-µm diameter multi-mode solid-core InF_3 fiber. The optical fibers are secured to kinematic optic mounts fastened to aluminum slip plate positioners, which together enable five degrees of freedom (X-, Y- and Z- translation, pitch, and yaw) for fine-tuning of the optical alignment. The schematic on the right of Fig. 1 shows the major photonic elements that interface with the exhaust sensor module and are located on a mobile breadboard away from the harsh combustion environment, a configuration enabled by the complete fiber-coupling system. The output beams of the QCL and ICL are each coupled into the single-mode fibers with fiberport alignment stages. The transmitted beams carried by the multi-mode fibers are focused on to two photovoltaic detectors (Vigo PVI-4TE-5) by CaF_2 plano-convex lenses mounted to alignment stages that also hold the aspheric fiber collimation packages and narrow-bandpass spectral filters to isolate the laser radiation from the thermal emission of the combustion gases.

The integration of the sensor module into the existing engine exhaust system of the test engine (detailed in Sec. 3) involved replacing the stock exhaust pipe with a custom-fabricated exhaust system, shown in the center of Fig. 1. A pipe expander mounted to the exhaust port expands the flow diameter from 27 mm to 50 mm while retaining the original O_2 sensor. A flexible pipe coupling connects the pipe expander to the exhaust sensor module while damping engine vibrations. This setup places the optical measurement location 26 cm downstream of the exhaust valve. A gas sampling port 5.5 cm downstream of the optical measurement is used to siphon exhaust gases to an emissions gas analyzer, detailed in Sec. 3. Downstream of the sensor module, the flow diameter is reduced to 27 mm for mating with the stock muffler and catalytic-converter assembly. This maintains emissions compliance of the engine after integration of the optical diagnostics. This modified exhaust system is secured with vibration-damping

TABLE 1: ENGINE SPECIFICATIONS

Model	Genconnex Honda EU7000is
IC engine	GX390T2
Cycle	4-stroke
Bore x Stroke	88 x 64 mm
Displacement	389 cm^3
Compression ratio	8.2:1
Cylinders	1
Valves per cylinder	2
Engine speed	3,300 rpm
Fuel	Natural gas
Equivalence ratio	1
Rated output	5.5 kW
Fueling method	Carburetor
Ignition method	Spark ignition
Ignition timing	Fixed at constant load

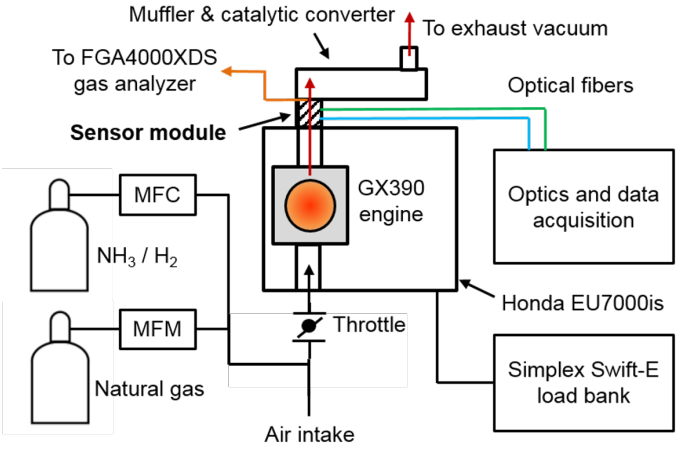

FIGURE 3: EXPERIMENTAL SETUP FOR TESTING WITH THE EU7000IS GENERATOR.

mounts to a support structure added to the engine frame for minimal increase of the engine footprint and retention of the original wheel-mounting and mobility.

By integrating the sensor in-stream with close proximity to the exhaust valve, exhaust gas transit time is short and results in minimal latency relative to combustion. This latency or exhaust gas transit time can be estimated with some simplifying assumptions. First, during the initial opening of the exhaust valve, or blowdown phase, the pressure differential between the high-pressure cylinder and the low-pressure exhaust pipe leads to choked flow across the valve [24]. Second, in-cylinder gas properties including the specific heat ratio can be estimated from combustion simulations. Lastly, with changing cross-sectional areas between the valve and sensor location, gas expansion can be approximated with quasi-1D compressible flow relations. For the test engine used in this work, when assuming 1 mm valve lift and choked flow through the exhaust valve with measured gas properties, in-cylinder combustion gases travel through the modified exhaust pipe and reach the optical line-of-sight within an estimated 7 ms. This corresponds to a conservative estimate of average gas velocity of approximately 40 m/s for the leading edge of the exhaust impulse. Notably, commercial exhaust gas analyzers that rely on gas sampling (and pre-conditioning) from the exhaust stream involve much longer gas transit times on the order of seconds or longer. In-situ measurements using laser absorption reduce the sensor latency due to gas transit from second-scale to ms-scale and on the same order of magnitude as the engine piston motion, which is critical for fast control schemes.

3. EXPERIMENTAL SETUP

The engine selected for demonstration with the developed laser absorption sensor is a Honda EU7000is generator driven by a single-cylinder SI engine (GX390T2) originally designed for gasoline but modified for natural gas-fueling by Genconnex. This is a commercially-available, EPA-certified engine representing the target application for a fast-response exhaust sensor integrated with real-time control for practical power generation. Table 1 lists specifications of the test engine. Aside from the exhaust system modifications detailed in Sec. 2.3 to incorporate the LAS sensor module, the engine is maintained in its original configuration. While originally controlled by electronic fuel injection, the natural gas conversion now relies on a pressure regulator and orifice to introduce fuel into the intake pipe upstream of the throttle valve. The engine electronic control unit (ECU) adjusts the throttle valve automatically to increase the amount of fuel/air mixture supplied to the engine to match the required power output while remaining at a constant 3,300 rpm. The ECU also adjusts spark timing based on the load applied to the generator and a predetermined engine map. The O_2 sensor is required for engine operation; however, it does not affect the ignition timing. The overhead intake and exhaust valves are pushrod-driven and have fixed valve lift profiles across the engine operating range.

The experimental setup for this investigation is shown in Fig. 3. The fuel is supplied by tanks of compressed natural gas, anhydrous ammonia, and hydrogen. Natural gas flowrate is monitored by a thermal-based mass flow meter (Omega FMA 1800) with an accuracy of ±1% of the full scale (50 slm N_2 equivalent). Blending of the natural gas with either NH_3 or H_2 is accomplished with a thermal-based mass flow controller (MKS GE50A) with an accuracy of ±0.2 % of the full scale (20 slm N_2 equivalent) for the flowrates used in this study. The fuel blending manifold connects to a 3 m long fuel hose leading to the EU7000is fuel intake. The engine exhaust is connected to a vacuum pump system to safely evacuate the gases from the laboratory. A portable resistive load bank (Simplex Swift-e) with a 10-kW capacity is used to apply the desired electrical load to the generator.

A mobile cart next to the test engine holds the breadboard-mounted photonics along with all other optoelectronics and the data acquisition system (National Instruments PXI-6115) controlled through LabVIEW. The optical fibers run between the cart-mounted breadboard and the exhaust sensor module during engine firing. A portion of the exhaust gas is siphoned off from the gas sampling port and transported through a 8 m long sampling tube to an exhaust gas analyzer (Infrared Industries FGA4000XDS). The gas analyzer measures CO and NO_x con-

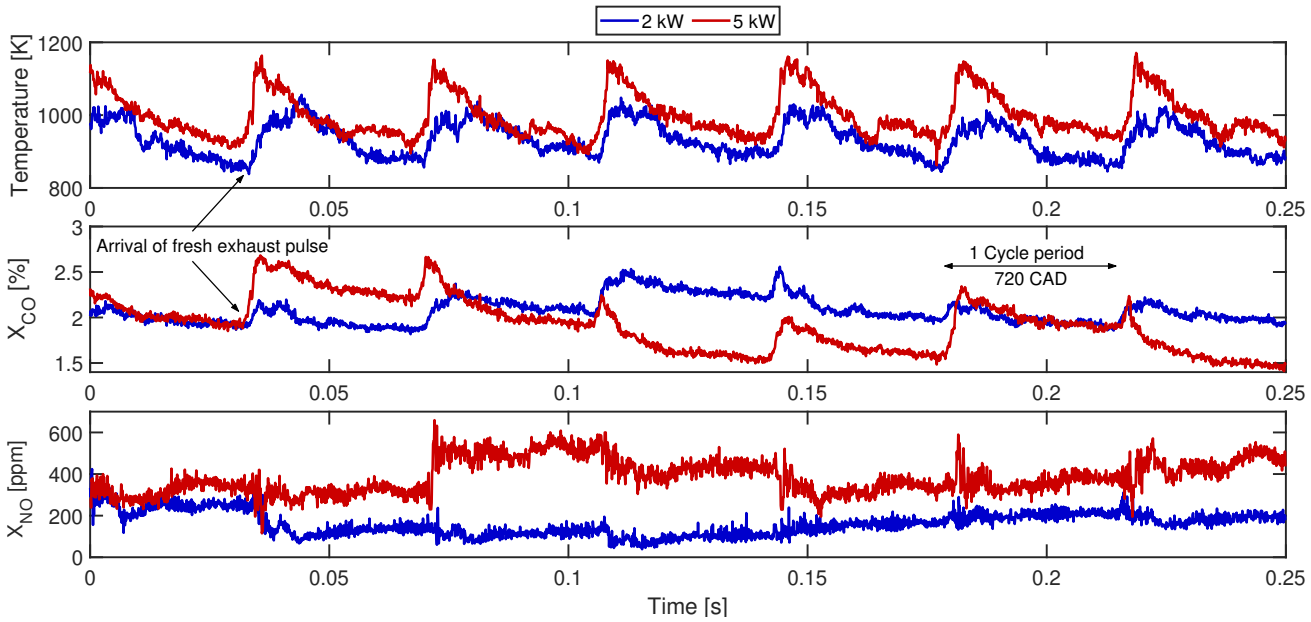

FIGURE 4: CYCLE-RESOLVED MEASUREMENTS OF EXHAUST GAS TEMPERATURE, CARBON MONOXIDE, AND NITRIC OXIDE. ENGINE RUNNING ON PURE NATURAL GAS AT 3,300 RPM AND TWO APPLIED LOAD CONDITIONS, 2 AND 5 KW.

centrations with an accuracy of 0.1% and 50 ppm, respectively. The analyzer relies on a NDIR sensor for the CO measurement and an EC sensor for NO_x, with a response time of 2 s.

4. RESULTS

4.1 Cycle-resolved Exhaust Sensing

The capability of the developed laser absorption sensor was first tested on the GX390T2 engine fueled with pure natural gas under varying load conditions. With the LAS temporal resolution of 0.1 ms and the engine operating at its standard 3,300 rpm (or cycle frequency of 27.5 Hz), this corresponds to 364 data points per cycle or a resolution better than 2 crank angle degrees (CAD). Figure 4 shows sample measurements captured in the engine exhaust at both high and low load. The temperature trace shows clear cyclic variation at the engine frequency of 27.5 Hz. The sharp increase corresponds to fresh exhaust gas traveling through the sensor line of sight when the exhaust valve opens at the beginning of the engine exhaust stroke. Within individual 36 ms cycles at 5 kW load, peak temperature consistently reaches over 1150 K and decreases by over 200 K due to expansion and cooling of the combustion gases as the cylinder depressurizes. Higher temperatures are consistently observed at 5-kW operation compared to the 2-kW operation, as expected due to increased reactant initial pressure and subsequent in-cylinder combustion temperatures. Consecutive exhaust-pulse temperatures for the same condition show consistent profile characteristics and peak temperatures, with fluctuations likely due to inhomogeneity in combustion and transport out of the cylinder. The sensor similarly captures the cycle-resolved characteristics of CO and NO exhaust emissions which are highly dynamic in this engine. The measured CO mole fraction mirrors the intra-cycle peak and decay of measured temperature. This could potentially be due to the retrofitted nature of the test engine which has not advanced the spark timing to account for slower natural gas flame speeds

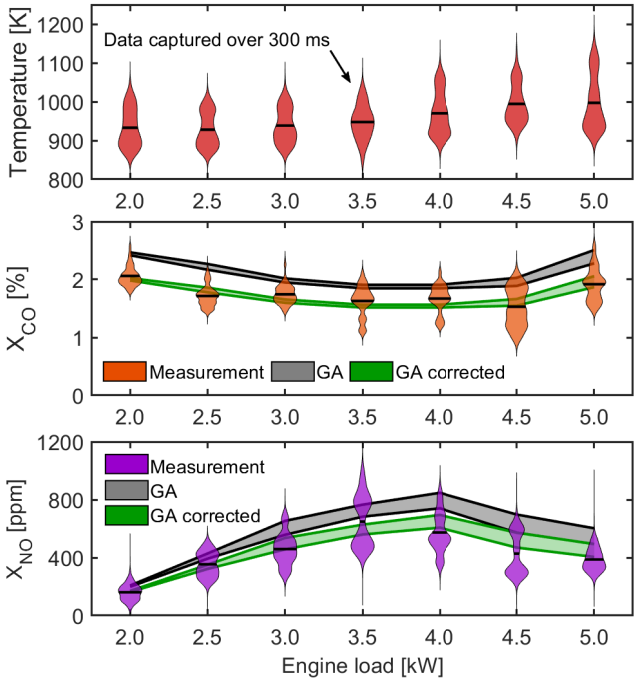

FIGURE 5: FROM TOP TO BOTTOM: TEMPERATURE, CARBON MONOXIDE CONCENTRATION, AND NITRIC OXIDE CONCENTRATION MEASURED IN THE EXHAUST GAS FROM 2- TO 5-KW LOADS. ENGINE RUNNING ON PURE NATURAL GAS WITH SIMULTANEOUS SAMPLING WITH THE FGA4000XDS GAS ANALYZER (GA). ANALYZER READOUT DATA SHOWN IN GREY, WITH DATA CORRECTED FOR LOSS IN WATER CONCENTRATION SHOWN IN GREEN. SOLID BLACK LINES WITHIN VIOLIN PLOTS REPRESENT MEAN VALUES.

compared to gasoline. The required spark advance can reach up to 10 CAD [2], and the omission of this adjustment could lead to the combustion reaction persisting after the exhaust valve opens which is supported by the observation of CH emission through the sapphire windows during engine firing. A different trend is observed in the measured NO mole fraction, where intra-cycle variations are less significant compared to the cycle-averaged concentrations. This may suggest that the majority of its formation occurs earlier in the expansion stroke, with remaining temporal evolution potentially due to chemistry in the exhaust pipe or heterogeneous distribution of NO in the cylinder.

While measurement traces of CO and NO exhibit a certain degree of intra-cycle variation, they mostly show an exceptionally high cycle-to-cycle variation at all load conditions despite the relative consistency in measured temperature. Between the two conditions in Fig. 4, there is little difference in mean CO concentration observed in the exhaust, although the data suggest cycle-to-cycle variation is higher during 5-kW operation. Within the 250-ms period presented in Fig. 4 for a 5-kW load, the cycle-average CO concentration reaches a maximum of 2.4% and a minimum of 1.7%. Similar cycle-to-cycle variations are encountered in the NO exhaust with maximum and minimum emissions averages of 510 and 310 ppm. These combustion inconsistencies are commonly observed in SI natural gas engines, especially those retrofitted from gasoline engines, but cannot be resolved by conventional exhaust gas analyzers.

The effect of applied load on measured exhaust conditions is illustrated further in Fig. 5, containing data captured over a 300-ms measurement interval or approximately 8 engine cycles. The data distributions are represented by violin plots which are wider for higher statistical occurrence. As load increases, both mean and peak temperatures increase steadily up to ~1000 K and ~1200 K, respectively. The measured mole fraction shows more dynamic behavior across the load range, with CO and NO exhibiting inverse dependencies. Minimum CO emissions occur in the 3.0–4.5 kW range, with those same conditions corresponding to peak NO production. This load dependence is expected in SI engines with limited adaptability and the need to strike a compromise across the operating range [24].

Gas analyzer readings are displayed in Fig. 5, with the grey shaded region representing the spread of readout values observed over a 30-s interval. The analyzer captures the same trends across the load range visible in the LAS measurements, and agrees reasonably well in magnitude, although on average displays slightly higher concentrations across the range (~15%). One noteworthy difference between the exhaust sensors is that the gas analyzer relies on a mass-weighted average measurement while LAS uses a non-temporally averaged line-of-sight measurement decoupled from exhaust mass flow rate. Furthermore, the gas analyzer NO_x sensor is sensitive to not just NO, but also NO_2, which can account for >10% of total NO_x emissions; this percentage increases with elevated levels of NO_x [25]. With the gas analyzer separated from the exhaust by 8 m of tubing, any chemistry occurring after the exhaust gases pass the optical measurement location can lead to discrepancies in both the measured CO and NO concentrations. Most significantly, the gas analyzer includes a filter for removing water vapor prior to exhaust gas measurement. Water concentration can be significant in this case, ~18% in stoichiometric natural gas combustion, and so correcting for this loss in exhaust gas content yields data shown in green in Fig. 5. These data more closely agree with those of the LAS sensor which is deployed in the untreated exhaust stream where water vapor is still present. It should be noted that the gas analyzer was calibrated with a certified emissions mixture prior to testing.

The most significant difference in the two emissions sensors is the capture of intra-cycle and cycle-to-cycle trends with the LAS sensor, which enables additional dimensions of analysis critical for real-time engine optimization and control applications. According to the gas analyzer reading, CO exhaust varies from 1.9% to 2.5% across all loads. This 0.6% CO variation is lower than the amplitudes measured by the LAS sensor within a single 300-ms period, spanning from 1% to 2.2% CO for the 3.5–4.5 kW loads. The same observation can be made regarding the NO measurements at each load, with typical 250–800 ppm variations measured by LAS. This highlights a high degree of combustion inconsistency in this commercially-available, EPA-certified engine that is undetected by the gas analyzer. It is notable that the regulated emissions generally exhibit more cycle-to-cycle variation than the measured temperature, indicating the high sensitivity of species formation to operating conditions in this test engine. The high-bandwidth data provide a means to reduce variation through systematic engine refinement, particularly if coupled with real-time control. One such example is the implementation of throttling with a variable lift intake valve. This technique increases fuel/air mixing and turbulence, promoting (i) homogeneous combustion, (ii) higher burning velocities, and (iii) more consistent cycle-to-cycle combustion. Throttling can be tuned in real-time and across the entire operating range of the engine and has been shown to reduce brake-specific fuel consumption by up to 10% [26].

The uncertainty in the measured temperature and mole fraction from the LAS sensor was calculated via the method put forth in Nair et al. [27] for scanned-wavelength direct laser absorption experiments and based on the Taylor series method of uncertainty propagation. This uncertainty accounts for noise in the measured raw intensities and subsequent extraction of absorbance areas in addition to uncertainty in physical parameters used to determine temperature and mole fraction through Eqs. 1 & 2, including pressure, pathlength, and tabulated spectroscopic parameters. The temperature uncertainty is dominated by the uncertainty in the measured absorbance area of the weaker P(1,14) transition of CO, and the maximum uncertainties are observed at engine operating conditions associated with low exhaust temperatures and low CO emissions. During standard operation with natural gas fuel, temperature uncertainty lies between 25 K and 31 K with the larger uncertainty corresponding to the minimum intra-cycle temperatures. Maximum uncertainties are reached during 10% NH_3/NG fueling (see Sec. 4.2) and range from 40 K to 55 K. The P(0,20) absorption remains high across all operating conditions and leads to a more consistent uncertainty in measured CO mole fraction of 2.9% of the measured value. The uncertainty in NO mole fraction is dependent on engine operating conditions and the large range in resulting NO emissions. An uncertainty of 26 ppm corresponds to minimal NO production

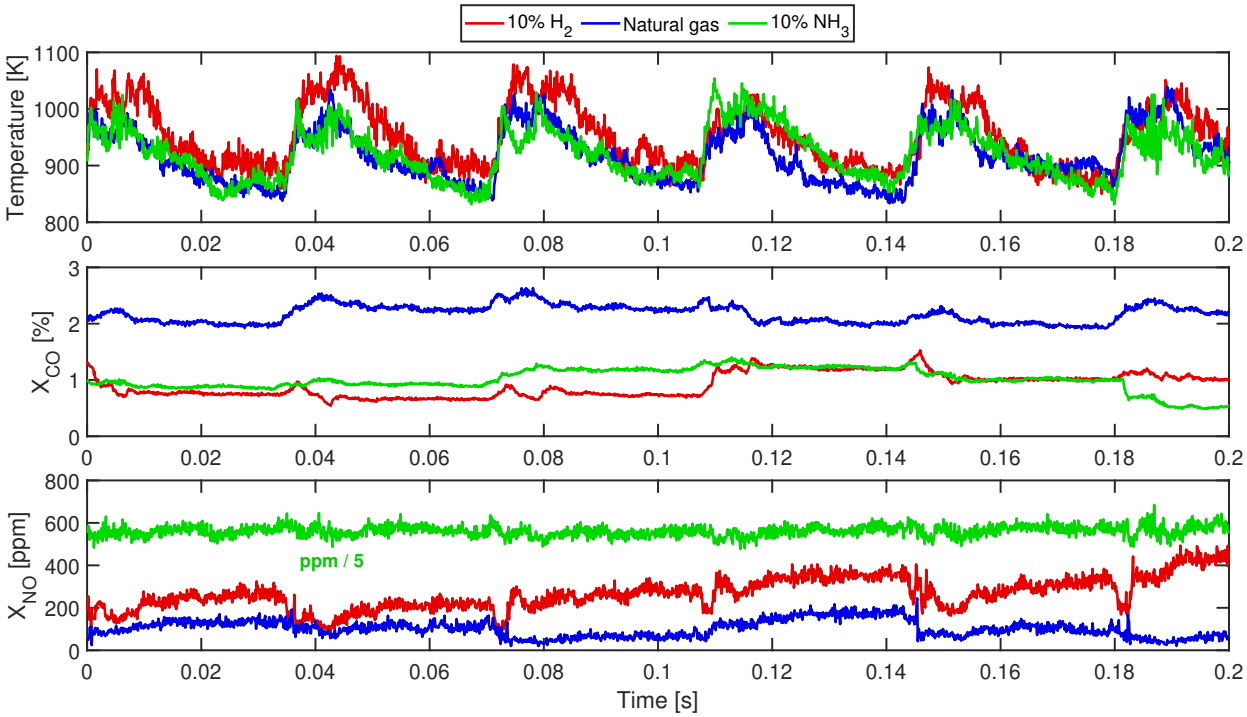

FIGURE 6: CYCLE-RESOLVED MEASUREMENTS OF EXHAUST GAS TEMPERATURE, CARBON MONOXIDE, AND NITRIC OXIDE. ENGINE RUNNING WITH 2 KW APPLIED LOAD AND THREE FUEL CONDITIONS: 100% NATURAL GAS, NATURAL GAS WITH 10 VOL. % AMMONIA, AND NATURAL GAS WITH 10 VOL. % HYDROGEN. NITRIC OXIDE EMISSIONS FOR 10% NH_3 FUELING ARE SCALED FOR PRESENTATION.

(<100 ppm) at low load and pure natural gas fueling, whereas uncertainty at 10% NH_3/NG fueling and maximum NO production (>3400 ppm) is approximately 180 ppm. These uncertainties translate to detection limits (1σ) of 0.07% and 26 ppm for CO and NO mole fraction, respectively.

4.2 Polyfuel Emissions Analysis

The application of the LAS exhaust sensor for polyfuel IC engines was investigated by operating the test engine with low-carbon fuel blends of natural gas mixed with NH_3 and H_2 at concentrations up to 10% by volume. Figure 6 shows cycle-resolved exhaust measurements of select blends compared to pure natural gas fueling. Across the fuel blending matrix, applied load was kept constant at 2 kW, resulting in consistent ignition timing. The measured temperature remains largely similar between the three fuels even at 10% blending, with slightly higher temperatures observed in individual H_2-enriched cycles due to the higher flame temperatures of H_2 combustion [28].

The effect of NH_3 and H_2 addition in this particular engine is much more drastic for the CO and NO emissions. Both additives reduced CO emissions by approximately a factor of 2 at 10% blending concentrations. There is a relatively small difference in CO reduction between H_2/NG and NH_3/NG blends in these cases, and neither blend shows a substantial change in the cycle-to-cycle consistency. Emissions of NO, however, show stark differences between the two blends. H_2 addition led to an appreciable increase in NO production by a factor of 2 over pure natural gas, however the NH_3/NG blending resulted in an order of magnitude increase. Additionally, the cycle-to-cycle consistency of NO emissions was

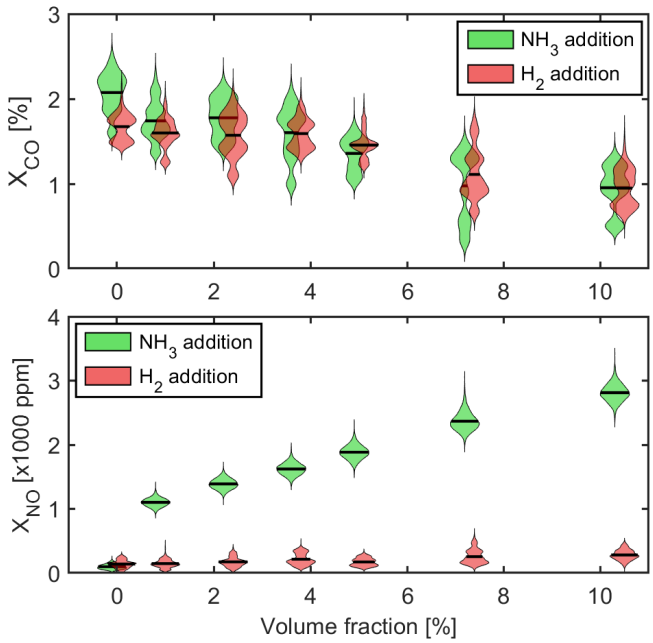

FIGURE 7: MEASURED EXHAUST CO CONCENTRATION *(TOP)* AND NO CONCENTRATION *(BOTTOM)*, COLLECTED OVER 300-MS INTERVAL. ENGINE LOAD IS 2-KW AND THE FUEL IS NATURAL GAS BLENDED WITH VARYING CONCENTRATIONS OF EITHER NH_3 OR H_2. VOLUME FRACTIONS ARE MATCHED BETWEEN THE DIFFERENT BLENDING CONSTITUENTS, WITH DATA SHOWN OFFSET FOR VISIBILITY.

noticeably greater during NH_3/NG fueling.

The measured emissions of the test engine fueled with these alternative blends as a function of volume fraction is displayed in Fig. 7. Both H_2 and NH_3 addition led to suppression of CO emissions at similar magnitudes. However, H_2/NG blends far outperformed NH_3/NG for minimizing NO emissions. The trends in NH_3 blends corroborate those reported by Oh et al., who reported mild variations in CO emissions and significant increases in NO emissions within 0–10% NH_3 addition while keeping NH_3 slip low [29]. It should be noted that the tests presented in this work were performed at low loads due to safety concerns fueling with premixed H_2/NG mixtures, including the possibility of flashback into the intake pipe upon intake valve opening events. Had the tests been performed at higher loads, then the increase in NO formation with increasing H_2 volume fraction may be more appreciable due to the likely increased in-cylinder combustion temperatures.

The trends of Fig. 7 suggest that at these conditions, the reduction in CO emissions is largely driven by the reduced carbon input and that the chemical effect of NH_3 or H_2 addition have similar impact (within the 10% addition). The reduction of CO emissions for H_2 blends was observed in a previous study by Aksu et al. and solely attributed to the reduction of carbon input in the fuel stream [30]. The CO exhaust is, however, marked here with a factor-of-two reduction (~2% to ~1%) while NG intake is diminished by only 10%. Thus, the reduced CO emissions cannot solely be attributed to the decreased natural gas intake. The similarity of H_2 and NH_3 blends is, upon a first order analysis, unsurprising given that NH_3 is essentially an H_2 carrier and, at high temperature, undergoes H-abstraction associated with H_2 production (among others) [31, 32]:

$$\begin{aligned} NH_3 + O_2 &\longrightarrow NH_2 + HO_2 \\ NH_3 + OH &\longrightarrow NH_2 + H_2O \\ NH_3 + H &\longrightarrow NH_2 + H_2 \end{aligned} \qquad \text{(R1)}$$

Therefore, CH_4 combustion is likely acting as a trigger for NH_3 splitting via the generation of H and OH radicals that accelerate Reac. (R1), generate H_2, and may explain the similarities between the two blends. However, the differences in NO production between the blends can be attributed to different mechanisms. While H_2 combustion often leads to increased thermal NO_x production through higher combustion temperatures, in ammonia combustion NO_x formation is typically governed by fuel NO_x via the HNO pathway, $NH_3 \rightarrow NH_2 \rightarrow HNO \rightarrow NO$ [33]. The measurement results suggest that at this operating condition, fuel NO_x is much more dominant than thermal NO_x. A full chemical kinetics investigation of H_2/NH_3/NG blends is beyond the scope of this paper, however.

The exhaust behaviors observed during polyfuel operation provide insight into paths for further combustion optimization in this engine. Hydrogen-enrichment has demonstrated value in improving combustion stability and efficiency in natural gas SI engines through increased flame speed and radical generation even at 10% H_2 in natural gas [2, 34]. However, in this study, we observed no significant improvement on cycle-to-cycle consistency due to hydrogen addition. The adjustment of spark timing and additional turbulence and mixing through intake valve variation through real-time control can be used to maximize the benefit of H_2 addition while monitoring thermal NO_x generation. Incorporating NH_3 into NG or H_2 fueling presents additional challenges due to low flame speeds and high fuel-NO_x emissions [29]. The incorporation of tri-fuel operation and control over on-board NH_3 cracking with feedback control informed by real-time emissions measurements can aid to minimize NO_x formation through suppression of the HNO pathway while promoting oxidation of alternatively generated N_2O [4, 5, 33, 35]. The engine also displayed a dependence of exhaust emissions on ambient conditions on the order of 10-20%, as evident with the difference in 0% blending cases between the NH_3/NG and H_2/NG datasets in Fig. 7. For practical engine applications, operating environments can vary greatly due to seasonal or geographic changes, day-to-day weather, and time of day. To ensure optimum engine operation for all conditions, the ability of the sensor to resolve these differences across a range of relevant timescales in exhaust emissions enhances the ability of any control system to adapt the system operation.

5. CONCLUSION

An in-situ laser absorption sensor has been developed for cycle-resolved measurements of exhaust gas properties in production IC engines and demonstrates the potential impact of high-speed, quantitative LAS exhaust sensors for real-world implementation. In this work, the LAS sensor captured intra-cycle, cycle-to-cycle, and engine load-dependent variation of CO, NO, and temperature in the exhaust of an EPA-compliant natural gas-fueled, Otto-cycle engine. This capability revealed combustion inefficiencies and inconsistencies associated with natural gas spark-ignition engines, and showed that NO and CO cycle-to-cycle emission variability is significant. The cycle-resolution was enabled by locating the exhaust sensor in-line with minimal distance from the engine exhaust valve leading to a reduction in sensor latency by 3 orders of magnitude over commercial on-line analyzer systems. The close-coupling of the sensor was achieved through a ruggedized optomechanical design that enabled prolonged operation (>10 hours) at the sustained high temperatures (>1000 K) near the exhaust valve without any wear or deterioration of the sensor module. This novel sensor capability provides a quantitative, time-resolved capture of exhaust dynamics that is currently unavailable for production engines.

The utility of the sensor in polyfuel applications was demonstrated by capturing the response of the test engine to low-carbon natural gas blends incorporating NH_3 and H_2. At low load, both blends similarly halved CO exhaust for only 10% admixture. A differing response was observed in the NO emissions, with H_2 and NH_3 addition leading to a factor of 2 and an order of magnitude increase, respectively. Cycle-to-cycle combustion variability was largely unaffected from blending in this study. Low detection limits of 0.07% CO and 25 ppm NO, coupled with a large dynamic range, enabled analysis of significantly different fuel chemistry in these polyfuel blends while remaining sensitive to cycle-level inconsistencies. It is expected that the combined durability, low-latency, and quantitative value of the developed LAS sensor will enable more direct and rapid optimization of low-carbon polyfuel

combustion in production IC engine systems.

ACKNOWLEDGMENTS

The work presented here was supported by Southern California Edison (Award no. 20181588). KKS acknowledges support through the Department of Defense National Defense Science and Engineering Graduate (NDSEG) fellowship. Additional support was provided by Tim and Karen Strelitz. SE acknowledges support through the UCLA Undergraduate Research Fellows Program and Undergraduate Research Center Sciences Summer Program. The authors thank Professor D.I. Pineda and Dr. A.P. Nair for helpful advice and for reviewing the manuscript.

REFERENCES

[1] U.S. EPA. "Inventory of U. S. GHG Emissions and Sinks." Technical Report No. EPA 430-R-22-003. 2022.

[2] Korakianitis, T., Namasivayam, A.M. and Crookes, R.J. "Natural-gas fueled spark-ignition (SI) and compression-ignition (CI) engine performance and emissions." *Progress in Energy and Combustion Science* Vol. 37 No. 1 (2011): pp. 89–112. DOI 10.1016/j.pecs.2010.04.002.

[3] Chiong, Meng Choung, Chong, Cheng Tung, Ng, Jo Han, Mashruk, Syed, Chong, William Woei Fong, Samiran, Nor Afzanizam, Mong, Guo Ren and Valera-Medina, Agustin. "Advancements of combustion technologies in the ammonia-fuelled engines." *Energy Conversion and Management* Vol. 244 No. April (2021): p. 114460. DOI 10.1016/j.enconman.2021.114460.

[4] Mercier, A., Mounaïm-Rousselle, C., Brequigny, P., Bouriot, J. and Dumand, C. "Improvement of SI engine combustion with ammonia as fuel: Effect of ammonia dissociation prior to combustion." *Fuel Communications* Vol. 11 No. December 2021 (2022): p. 100058. DOI 10.1016/j.jfueco.2022.100058.

[5] Lhuillier, Charles, Brequigny, Pierre, Contino, Francesco and Mounaïm-Rousselle, Christine. "Experimental study on ammonia/hydrogen/air combustion in spark ignition engine conditions." *Fuel* Vol. 269 No. February (2020): p. 117448. DOI 10.1016/j.fuel.2020.117448.

[6] Oh, Sechul, Park, Cheolwoong, Kim, Seonyeob, Kim, Yongrae, Choi, Young and Kim, Changgi. "Natural gas–ammonia dual-fuel combustion in spark-ignited engine with various air–fuel ratios and split ratios of ammonia under part load condition." *Fuel* Vol. 290 No. January (2021): p. 120095. DOI 10.1016/j.fuel.2020.120095.

[7] Moreno, F., Muñoz, M., Arroyo, J, Magén, O., Monné, C. and Suelves, I. "Efficiency and emissions in a vehicle spark ignition engine fueled with hydrogen and methane blends." *International Journal of Hydrogen Energy* Vol. 37 No. 15 (2012): pp. 11495–11503. DOI 10.1016/j.ijhydene.2012.04.012.

[8] Lou, Zheng and Zhu, Guoming. "Review of Advancement in Variable Valve Actuation of Internal Combustion Engines." *Applied Sciences* Vol. 10 No. 4 (2020): p. 1216. DOI 10.3390/app10041216.

[9] Spinelle, Laurent, Gerboles, Michel, Kok, Gertjan, Persijn, Stefan and Sauerwald, Tilman. "Review of Portable and Low-Cost Sensors for the Ambient Air Monitoring of Benzene and Other Volatile Organic Compounds." *Sensors* Vol. 17 No. 7 (2017): p. 1520. DOI 10.3390/s17071520.

[10] Niklas, Christian, Bauke, Stephan, Müller, Fabian, Golibrzuch, Kai, Wackerbarth, Hainer and Ctistis, Georgios. "Quantitative measurement of combustion gases in harsh environments using NDIR spectroscopy." *Journal of Sensors and Sensor Systems* Vol. 8 No. 1 (2019): pp. 123–132. DOI 10.5194/jsss-8-123-2019.

[11] Yoo, Jihyung, Prikhodko, Vitaly, Parks, James E., Perfetto, Anthony, Geckler, Sam and Partridge, William P. "Fast spatially resolved exhaust gas recirculation (EGR) distribution measurements in an internal combustion engine using absorption spectroscopy." *Applied Spectroscopy* Vol. 69 No. 9 (2015): pp. 1047–1058. DOI 10.1366/14-07796.

[12] Goldenstein, Christopher S., Spearrin, R.Mitchell, Jeffries, Jay B. and Hanson, Ronald K. "Infrared laser-absorption sensing for combustion gases." *Progress in Energy and Combustion Science* Vol. 60 (2017): pp. 132–176. DOI 10.1016/j.pecs.2016.12.002.

[13] Hanson, Ronald K., Spearrin, R. Mitchell and Goldenstein, Christopher S. *Spectroscopy and Optical Diagnostics for Gases*. Springer International Publishing, Cham (2016). DOI 10.1007/978-3-319-23252-2.

[14] Cho, Haeng Muk and He, Bang-quan. "Spark ignition natural gas engines—A review." *Energy Conversion and Management* Vol. 48 No. 2 (2007): pp. 608–618. DOI 10.1016/j.enconman.2006.05.023.

[15] Spearrin, R. M., Goldenstein, C. S., Schultz, I. A., Jeffries, J. B. and Hanson, R. K. "Simultaneous sensing of temperature, CO, and CO2 in a scramjet combustor using quantum cascade laser absorption spectroscopy." *Applied Physics B: Lasers and Optics* Vol. 117 No. 2 (2014): pp. 689–698. DOI 10.1007/s00340-014-5884-0.

[16] Wei, Chuyu, Schwarm, Kevin K., Pineda, Daniel I. and Spearrin, R. Mitchell. "Volumetric laser absorption imaging of temperature, CO and CO2 in laminar flames using 3D masked Tikhonov regularization." *Combustion and Flame* Vol. 224 (2021): pp. 239–247. DOI 10.1016/j.combustflame.2020.10.031.

[17] Diemel, O, Pareja, J, Dreizler, A and Wagner, S. "An interband cascade laser - based in situ absorption sensor for nitric oxide in combustion exhaust gases." *Applied Physics B* (2017): pp. 1–8DOI 10.1007/s00340-017-6741-8.

[18] Diemel, Oliver, Honza, Rene, Ding, Carl-philipp, Böhm, Benjamin and Wagner, Steven. "In situ sensor for cycle-resolved measurement of temperature and mole fractions in IC engine exhaust gases." *Proceedings of the Combustion Institute* Vol. 37 No. 2 (2019): pp. 1453–1460. DOI 10.1016/j.proci.2018.06.182.

[19] Rothman, L.S., Gordon, I.E., Barber, R.J., Dothe, H., Gamache, R.R., Goldman, A., Perevalov, V.I., Tashkun, S.A. and Tennyson, J. "HITEMP, the High-Temperature Molecular Spectroscopic Database." *Journal of Quantitative Spectroscopy and Radiative Transfer* Vol. 111 No. 15 (2010): pp. 2139–2150. DOI 10.1016/j.jqsrt.2010.05.001.

[20] Hargreaves, Robert J., Gordon, Iouli E., Rothman, Laurence S., Tashkun, Sergey A., Perevalov, Valery I., Lukashevskaya, Anastasiya A., Yurchenko, Sergey N., Tennyson, Jonathan and Müller, Holger S.P. "Spectroscopic line parameters of NO, NO2, and N2O for the HITEMP database." *Journal of Quantitative Spectroscopy and Radiative Transfer* Vol. 232 No. 2 (2019): pp. 35–53. DOI 10.1016/j.jqsrt.2019.04.040.

[21] Almodovar, Christopher A, Su, Wey-wey, Strand, Christopher L and Hanson, Ronald K. "R-branch line intensities and temperature-dependent line broadening and shift coefficients of the nitric oxide fundamental rovibrational band." *Journal of Quantitative Spectroscopy and Radiative Transfer* Vol. 239 (2019): p. 106612. DOI 10.1016/j.jqsrt.2019.106612.

[22] White, John U. "Long Optical Paths of Large Aperture." *Journal of the Optical Society of America* Vol. 32 No. 5 (1942): p. 285. DOI 10.1364/JOSA.32.000285.

[23] Hannan, Paul. "White cell design considerations." *Optical Engineering* Vol. 28 No. 11 (1989): pp. 1180–1184.

[24] Heywood, John B. *Internal Combustion Engine Fundamentals*, 2nd ed. McGraw-Hill Education (2018).

[25] Soltic, Patrik and Weilenmann, Martin. "NO2/NO emissions of gasoline passenger cars and light-duty trucks with Euro-2 emission standard." *Atmospheric Environment* Vol. 37 No. 37 (2003): pp. 5207–5216. DOI 10.1016/j.atmosenv.2003.05.003.

[26] Tripathy, Srinibas, Das, Abhimanyu and Srivastava, Dhananjay Kumar. "Electro-pneumatic variable valve actuation system for camless engine: Part II-fuel consumption improvement through un-throttled operation." *Energy* Vol. 193 (2020): p. 116741. DOI 10.1016/j.energy.2019.116741.

[27] Nair, Anil P, Lee, Daniel D, Pineda, Daniel I, Kriesel, Jason, Hargus, William A., Bennewitz, John W, Danczyk, Stephen A and Spearrin, R Mitchell. "MHz laser absorption spectroscopy via diplexed RF modulation for pressure, temperature, and species in rotating detonation rocket flows." *Applied Physics B* Vol. 126 No. 8 (2020): p. 138. DOI 10.1007/s00340-020-07483-8.

[28] Law, Chung K. *Combustion Physics*. Cambridge University Press, New York (2006).

[29] Oh, Sechul, Park, Cheolwoong, Kim, Seonyeob, Kim, Yongrae, Choi, Young and Kim, Changgi. "Natural gas–ammonia dual-fuel combustion in spark-ignited engine with various air–fuel ratios and split ratios of ammonia under part load condition." *Fuel* Vol. 290 No. December 2020 (2021): p. 120095. DOI 10.1016/j.fuel.2020.120095.

[30] Aksu, Cagdas, Kawahara, Nobuyuki, Tsuboi, Kazuya, Nanba, Shun, Tomita, Eiji and Kondo, Morio. "Effect of Hydrogen Concentration on Engine Performance, Exhaust Emissions and Operation Range of PREMIER Combustion in a Dual Fuel Gas Engine Using Methane-Hydrogen Mixtures." *SAE Technical Papers* Vol. 2015-Septe No. September. DOI 10.4271/2015-01-1792.

[31] Mathieu, Olivier and Petersen, Eric L. "Experimental and modeling study on the high-temperature oxidation of Ammonia and related NOx chemistry." *Combustion and Flame* Vol. 162 No. 3 (2015): pp. 554–570. DOI 10.1016/j.combustflame.2014.08.022.

[32] Otomo, Junichiro, Koshi, Mitsuo, Mitsumori, Teruo, Iwasaki, Hiroshi and Yamada, Koichi. "Chemical kinetic modeling of ammonia oxidation with improved reaction mechanism for ammonia/air and ammonia/hydrogen/air combustion." *International Journal of Hydrogen Energy* Vol. 43 No. 5 (2018): pp. 3004–3014. DOI 10.1016/j.ijhydene.2017.12.066.

[33] Kobayashi, Hideaki, Hayakawa, Akihiro, Somarathne, K.D. Kunkuma A. and Okafor, Ekenechukwu C. "Science and technology of ammonia combustion." *Proceedings of the Combustion Institute* Vol. 37 No. 1 (2019): pp. 109–133. DOI 10.1016/j.proci.2018.09.029.

[34] Kahraman, Nafiz, Çeper, Bilge, Akansu, S. Orhan and Aydin, Kadir. "Investigation of combustion characteristics and emissions in a spark-ignition engine fuelled with natural gas-hydrogen blends." *International Journal of Hydrogen Energy* Vol. 34 No. 2 (2009): pp. 1026–1034. DOI 10.1016/j.ijhydene.2008.10.075.

[35] Miller, James A., Smooke, Mitchell D., Green, Robert M. and Kee, Robert J. "Kinetic Modeling of the Oxidation of Ammonia in Flames." *Combustion Science and Technology* Vol. 34 No. 1-6 (1983): pp. 149–176. DOI 10.1080/00102208308923691.